Neutrosophic Sets and Systems, Vol. 53, 2023
University of New Mexico

New Control Chart Based On Neutrosophic Maxwell Distribution with Decision Making Applications

Faisal Shah[1], Muhammad Aslam[1], Zahid Khan[2]*

[1] Department of Mathematics and Statistics, Riphah International University, Islamabad 45210, Pakistan; faisal.shah@uoh.edu.pk ; m.aslam@riphah.edu.pk

[2] Department of Mathematics and Statistics, Hazara University Mansehra, Pakistan; zahidkhan@hu.edu.pk

* Correspondence: zahidkhan@hu.edu.pk

Abstract: The neutrosophic approach is a potential area to provide a novel framework for dealing with uncertain data. This study aims to introduce the neutrosophic Maxwell distribution $(\widetilde{\mathrm{MD}})$ for dealing with imprecise data. The proposed notions are presented in such a manner that the proposed model may be used in a variety of circumstances involving indeterminate, ambiguous, and fuzzy data. The suggested distribution is particularly useful in statistical process control (SPC) for processing uncertain values in data collection. The existing formation of $\mathrm{V_{SQ}}$-chart is incapable of addressing uncertainty on the quality variables being investigated. The notion of neutrosophic $\mathrm{V_{SQ}}$-chart $(\widetilde{\mathrm{V}}_{\mathrm{SQ}})$ is developed based on suggested neutrosophic distribution. The parameters of the suggested $\widetilde{\mathrm{V}}_{\mathrm{SQ}}$-chart and other performance indicators, such as neutrosophic power curve $(\widetilde{\mathrm{PC}})$, neutrosophic characteristic curve $(\widetilde{\mathrm{CC}})$ and neutrosophic run length $(\widetilde{\mathrm{RL}})$ are established. The performance of the $\widetilde{\mathrm{V}}_{\mathrm{SQ}}$-chart under uncertain environment is also compared to the performance of the conventional model. The comparative findings depict that the proposed $\widetilde{\mathrm{V}}_{\mathrm{SQ}}$-chart outperforms in consideration of neutrosophic indicators. Finally, the implementation procedure for real data on the COVID-19 incubation period is explored to support the theoretical part of the proposed model.

Keywords: Neutrosophic probability; Maxwell distribution; Maxwell control chart; Simulation; Estimation

1. INTRODUCTION

Statistical process control (SPC) is a set of statistical methods for process improvement and quality control. SPC is applied to observe and control a process to reduce the possibility of rework [1]. The ability to work at maximum capacity is made possible by monitoring and controlling the process [2]. SPC is a process for determining whether or not produced products satisfy the criteria and then adjusting the process to generate the desired proportion of conforming items [3]. The control chart is one of the most well-known SPC tools for observing and reducing the variation in the process. Because of many inherent causes, normal variation occurrence in closely every manufactured object is the best possible phenomenon [4]. The SPC is a standard approach that uses statistical techniques for estimating fluctuations in production or manufacturing process

parameters [5]. The role of a SPC is more significant in manufacturing industries [6]. This method is widely used to study the behaviour of processes and enhance their production [7]. SPC aims to detect irregularities in made items as early as feasible to stop the progression before defective products are made [8]. The Shewhart's model, developed by Walter A. Shewhart, is a popular predictive process tool that is simple to apply and comprehend [9]. The Shewhart control chart scheme is usually not recommended in service sectors and production operations where slight modifications can result in substantial monetary losses due to its ease of development and widespread use [10]. As a result, a chart of memory types that highly responsive to small shifts in study parameters. By contrast, most real-world systems can have uncertainties or indeterminacies [11]. Shewhart control charts cannot accurately identify a process if the process is ambiguous or essential quality characteristics are determined by human subjectivity [12]–[14]. As a result, problems are explained and modelled using fuzzy set theory. Research studies [15]–[17] reveal a simple application of fuzzy charts. On average, fuzzy-based control charts are more sensitive than traditional control charts [18]. The neutrosophic approach is a more general concept and provides a platform that combines a fuzzy concept set with the notion of a classical set [19]–[21]. The neutrosophic philosophy considers the existence of truth, false, and imprecise situations . The concept of neutrosophy is currently being used in various disciplines [22]. New application areas for SPC techniques are emerging, demanding further attention.

In a variety of real-world scenarios, the collected data may be ambiguous [23]. Various researchers use neutrosophical philosophy to address the problems of having incomplete data [24]–[29]. In the field of neutrosophic statistics, the traditional statistical methods have been comprehensive to address the management of data involving ambiguity. When the underlying data consists of incomplete, unclear, or uncertain data on quality characteristics, it is impossible to utilize a typical control chart technique. Numerous researchers such as [13], [16], [30], [31] have suggested statistical approaches that are linked with neutrosophic logic in the domains SPC [17]. When the premise of normality is seriously questioned, the use of commonly used control charts is far less appropriate [32]. The V_{SQ} is one of these approaches for dealing with nonnormality in quality data, which is best represented by the classical Maxwell model [33]. The Maxwell distribution is a statistical distribution that has sparked the interest of many scholars owing to its numerous practical applications [34], [35].

In this work, neutrosophic aspect of the Maxwell model with application domains in SPC is presented. The neutrosophic version of the V_{SQ}-chart that may handle the vague, incomplete or imprecise observations in underlying Maxwell quality characteristics is suggested.

The rest of the work is organized as follows: The notions of $\widetilde{MD}$ are first introduced in Section 2. Section 3 contains the proposed control chart based on $\widetilde{MD}$. The suggested neutrosophic design performance measure is provided in Section 4. Section 5 contains a comparative analysis of the $\widetilde{V}_{SQ}$-chart. An actual example of the useful execution of the suggested $\widetilde{V}_{SQ}$-chart is expounded in Section 6. Section 7 summarizes the key findings of the work.

2. STRUCTURE OF THE PROPOSED DISTRIBUTION

This section presents an overview of the suggested distribution and introduces it in a unified framework. The following definitions establish a connection between the proposed model and its applications in the neutrosophic framework.

Definition 1: The neutrosophic density function ($\widetilde{PDF}$) and Distribution function ($\widetilde{CDF}$) respectively of the $\widetilde{MD}$ with fuzziness in the scale parameter$\tilde{\vartheta}$are defined as:

$$f_N(t,\tilde{\vartheta}) = \sqrt{\left(\frac{2}{\pi}\right)}\tilde{\vartheta}^{-3}t^2 e^{-\frac{t^2}{2\tilde{\vartheta}^2}};\ \tilde{\vartheta} > 0, t > 0 \tag{1}$$

$$F_N(t,\tilde{\vartheta}) = \left(\frac{2}{\sqrt{\pi}}\right)\gamma\left[\frac{3}{2}, \frac{t^2}{2\tilde{\vartheta}^2}\right];\ \tilde{\vartheta} > 0, t > 0 \tag{2}$$

where $\tilde{\vartheta} = [\vartheta_1, \vartheta_u]$ and the neutrosophic random variable $\mathbf{T}$. In the framework of neutrosophic calculus, it is defined as the integral of the variable density over a specified range. The neutrosophic parameter $\tilde{\vartheta}$ denotes simply the scale factor whose different values result in a variety of neutrosophic curves of the proposed distribution. The graphs of $\widetilde{PDF}$ and $\widetilde{CDF}$ for a continuous random variable $\mathbf{T}$ with different neutrosophic values of the scale parameter are depicted in Figure 1 and Figure 2, respectively.

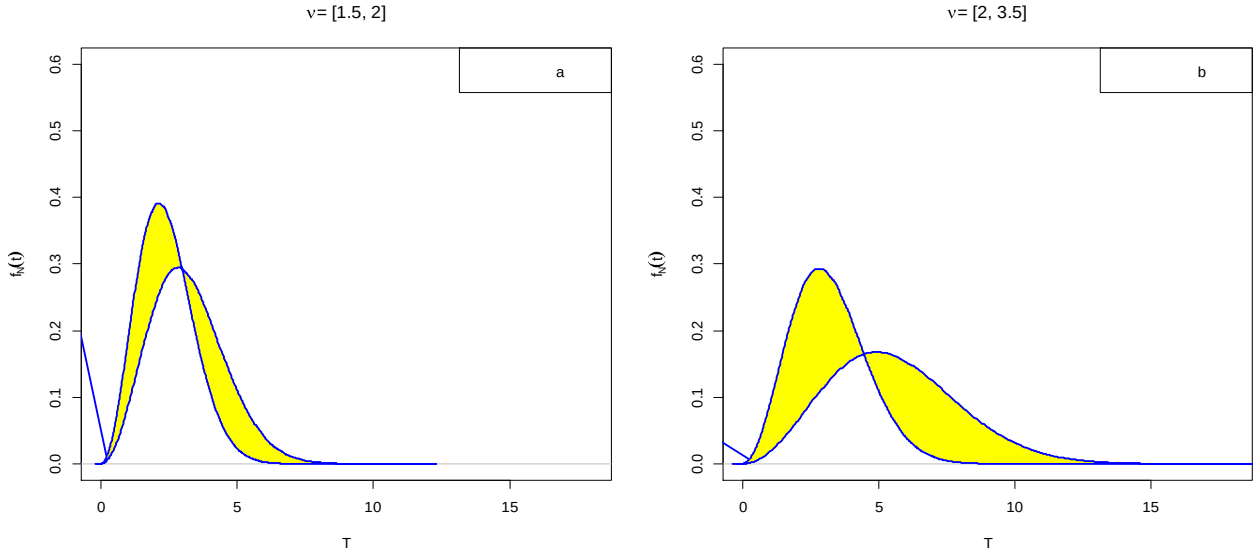

Figure 1. The $\widetilde{PDF}$ plots of the proposed model with (a) $\tilde{\vartheta} = [1.5, 2]$ and (b) $\tilde{\vartheta} = [2, 3.5]$

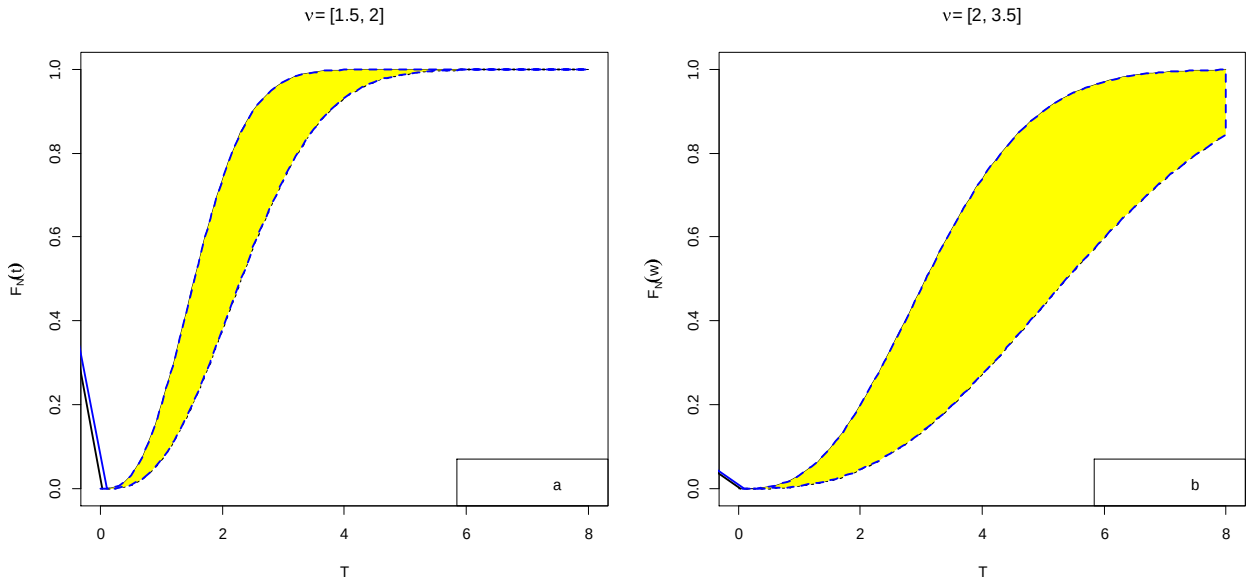

Figure 2. The $\widetilde{CDF}$ plots of the proposed model with (a) $\tilde{\vartheta} = [1.5, 2]$ and (b) $\tilde{\vartheta} = [2, 3.5]$

Figure 1 shows that the densities are asymmetric and skewed toward the right. In the neutrosophic framework, the density curve is represented by a thick layer rather than a single curve. The layer thickness (shaded region) corresponds to an indeterminacy part and total area under the sturdy curve equal to one due to completeness of $\widetilde{PDF}$. In addition, Figure 2 shows the overall behaviour of $\widetilde{CDF}$ which is right continuous and varies in the interval $[0,\ 1]$.

Definition 2 Mean and variance of the $\widetilde{\mathrm{MD}}$ are respectively given by

$$\tilde{\mu} = 2\tilde{\vartheta}\sqrt{\frac{2}{\pi}}, \text{ and } \tilde{\sigma}^2 = (3\pi - 8)\frac{\tilde{\vartheta}^2}{\pi}$$

Proof By definition

$$E(T) = \int_0^{\infty} t\ f_N(t)dt$$

$$= \int_0^{\infty} t\,[f_l(t), f_u(t)]dt$$

$$= \left[\int_0^{\infty} t\ f_l(t)dt, \int_0^{\infty} t\ f_u(t)dt\right]$$

$$= [2\tilde{\vartheta}_l\sqrt{\frac{2}{\pi}}\ ,\ 2\tilde{\vartheta}_u\sqrt{\frac{2}{\pi}}\,]$$

(3)

$= 2\breve{\vartheta}\sqrt{\frac{2}{\pi}}$, is the required mean value of the random variable T

Now the second raw moment of the $\widetilde{\mathrm{MD}}$ is given by:

$$E(T^2) = \int_0^{\infty} t^2\, f_N(t)dt$$

$$= \int_0^{\infty} t^2\, [\,f_l(t),\, f_u(t)]dt$$

$$= \left[\int_0^{\infty} t^2\, f_l(t)dt, \int_0^{\infty} t^2\, f_u(t)dt\right]$$

$$= [3\tilde{\vartheta}_l, \quad 3\tilde{\vartheta}_u]$$

$$E(T^2) = 3\tilde{\vartheta}^2$$

Thus the variance becomes

Now $\sigma^2{}_N(t) = E(T^2) - (E(T))^2 = [3\tilde{\vartheta}_l,\ 3\tilde{\vartheta}_u] - ([2\tilde{\vartheta}_l\sqrt{\frac{2}{\pi}}\ ,\ 2\tilde{\vartheta}_u\sqrt{\frac{2}{\pi}}\,])^2$

After simplifying, we get

$$= \left[(3\pi - 8)\frac{\tilde{\vartheta}_l{}^2}{\pi}\ , (3\pi - 8)\frac{\tilde{\vartheta}_u{}^2}{\pi}\right] \qquad (4)$$

Further neutrosophic measures of the proposed can be derived in a similar way using the neutrosophic calculus.

The Maxwell distribution is extensively used to describe wind speed data, communications data in signals processing, modelling of wind speed data, lifetimes of different objects in reliability studies, and noise factor modelling in magnetic imaging and SPC. With particularly focus on SPC, designing of new $\tilde{V}_{SQ}$. The chart based on the neutrosophic version of the Maxell model is described in the next section.

3. CONSTRUCTION OF CONTROL CHART

Assume that the desired quality attribute is given by Y and that it follows the neutrosophic form of the Maxwell model as described in (1). In most real-world circumstances, the value of the neutrosophic parameter $\check{\vartheta}$ is rarely known and usually estimated by the maximum likelihood (ML) approach. Let $y_{1N}, y_{2N}, y_{3N} \ldots \ldots . y_{\tilde{m}N}$ be the observed interval values sample from $\widetilde{\mathrm{MD}}$ with density function $f_N(y, \tilde{\vartheta})$. Assume the parameter $\tilde{\vartheta}$ is unknown in the defined distribution, then $\prod_{i=1}^{\tilde{m}} f_N(y_i, \tilde{\vartheta})$ be the joint probability of the observed sample.

Taking the logarithm of the product $\prod_{i=1}^{\tilde{m}} \phi_N(y_i, \tilde{\vartheta})$ provides log-likelihood as:

$$\xi_N(y_{iN}, \tilde{\vartheta}) = \frac{\tilde{m}}{2}\log\left(\frac{2}{\pi}\right) - 3\tilde{m}log\tilde{\vartheta} + log\prod_{i=1}^{\tilde{m}} {y_{iN}}^2 - \frac{\sum_{i=1}^{\tilde{m}} {y_{iN}}^2}{2\tilde{\vartheta}^2} \quad (5)$$

where $\tilde{m} = [m_l, m_u]$ is the neutrosophic sample size which turns to classical sample size when $m_l = m_u = m$

The ML estimate of the unknown $\tilde{\vartheta}$ is the value that maximizes $\xi_N(y, \tilde{\vartheta})$ i.e.,

$$\hat{\tilde{\vartheta}} = \max\left(\xi_N(y_{iN}, \tilde{\vartheta})\right)$$

The ML estimates, namely $\hat{\lambda}_N$ can be obtained by using the neutrosophic calculus as:

$$\frac{\delta\xi_N(y,\tilde{\vartheta})}{\delta\tilde{\vartheta}} = [\frac{\delta\xi_l(y_{il},\tilde{\vartheta}_l)}{\delta\tilde{\vartheta}_u}, \frac{\delta\xi_u(y_{iu},\tilde{\vartheta}_u)}{\delta\tilde{\vartheta}_l}] \quad (6)$$

where $\xi_l(y, \tilde{\vartheta}_l) = \frac{m_l}{2}\log\left(\frac{2}{\pi}\right) - 3\tilde{m}log\tilde{\vartheta}_l + log\prod_{i=1}^{m_l} {y_{il}}^2 - \frac{\sum_{i=1}^{m_l} {y_{il}}^2}{2{\tilde{\vartheta}_l}^2}$

and

$$\xi_u(y, \tilde{\vartheta}_u) = \frac{m_u}{2}\log\left(\frac{2}{\pi}\right) - 3nlog\tilde{\vartheta}_u + log\prod_{i=1}^{m_u} {y_{iu}}^2 - \frac{\sum_{i=1}^{m_u} {y_{iu}}^2}{2{\tilde{\vartheta}_u}^2}.$$

Simplification of (6) provides:

$$\frac{\delta\xi_N(y,\tilde{\vartheta})}{\delta\tilde{\vartheta}} = [\frac{-3m_l}{\tilde{\vartheta}_l} + \frac{\sum_{i=1}^{m_l} {y_{il}}^2}{{\tilde{\vartheta}_l}^3}, \frac{-3m_u}{\tilde{\vartheta}_u} + \frac{\sum_{i=1}^{m_u} {y_{iu}}^2}{{\tilde{\vartheta}_u}^3}] \quad (7)$$

Equating (7) to $[0, 0]$ yields:

$$\left[\hat{\tilde{\vartheta}}_l, \hat{\tilde{\vartheta}}_u\right] = \left[\sqrt{\frac{\sum_{i=1}^{m_l} {y_{il}}^2}{3m_l}}, \sqrt{\frac{\sum_{i=1}^{m_u} {y_{iu}}^2}{3m_u}}\right] = \sqrt{\frac{\sum_{i=1}^{\tilde{m}} {y_{iN}}^2}{3\tilde{m}}}$$

Thus

$\widehat{\tilde{\vartheta}} = \sqrt{\frac{\sum_{i=1}^{\tilde{m}} {y_{iN}}^2}{3\tilde{m}}}$ is the required ML estimator for the neutrosophic parameter of $\widetilde{\text{MD}}$.

For structuring the parameters of proposed $\tilde{V}_{SQ}$-chart, we have to establish the distribution of the $\widehat{\tilde{\vartheta}}$-estiamator. The chi ($\chi$) random variable Z with 3-degree of freedom (df) is associated with the estimator $\widehat{\tilde{\vartheta}}$ as follows [31]:

$$\widehat{\tilde{\vartheta}} = \frac{\sigma}{\sqrt{3m}} Z \tag{8}$$

It is now assumed that uncertain values of σ and m are provided instead of accurate values. Under neutrosophic environment expression (8) can be written as follows:

$$\widehat{\tilde{\vartheta}} = \frac{\sigma_N}{\sqrt{3\tilde{m}}} \tilde{Z} \tag{9}$$

where $\sigma_N = [\sigma_l, \sigma_u]$, $\tilde{m} = [m_l, m_u]$ and $\tilde{Z}$ is the neutrosophic chi (χ_N) a random variable with $3\tilde{m}$ degree of freedom. The skewed curve is a collective term for the χ distribution. The density plot of the χ_N variable with neutrosophic df is displayed in Figure 3.

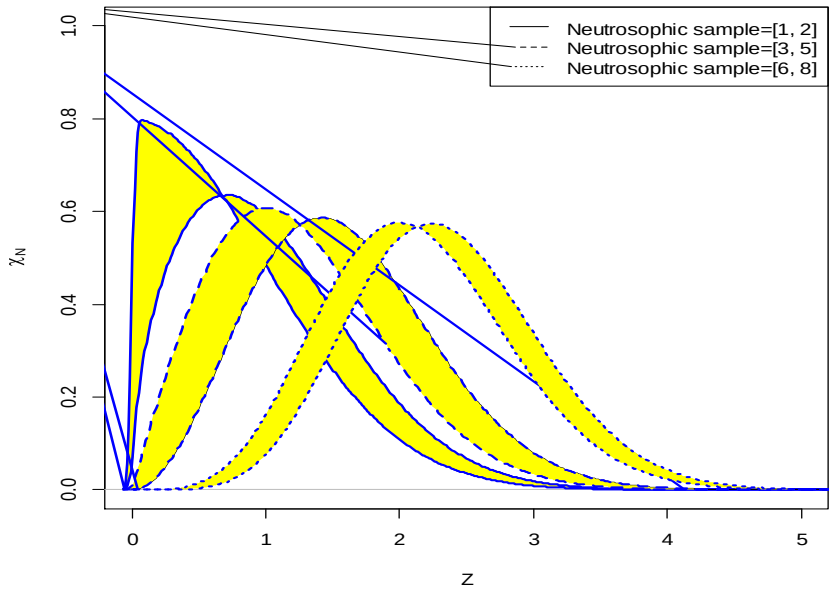

Figure 3. Probability curves of the χ_N random variable

Figure 3 is sketched to familiar with the neutrosophic form of the χ_N distribution for the case of various neutrosophic degrees of freedom. It is depicted from Figure 3 that distribution is skewed to the right for the lower degree of freedom. The distributional characteristics of the estimator $\widehat{\tilde{\vartheta}}$ using (9) can be established) as :

$$E\left(\widehat{\tilde{\vartheta}}\right) = \sigma_N \delta$$

$$V\left(\widehat{\tilde{\vartheta}}\right) = \sigma^2{}_N[1-\delta^2] \tag{10}$$

where $\delta = \sqrt{\left(\frac{2}{3\tilde{m}}\right)}\left(\frac{\Gamma\left(\frac{(3\tilde{m}+1)}{2}\right)}{\Gamma\left(\frac{3\tilde{m}}{2}\right)}\right)$ is an interval form of the neutrosophic constant and counts on $\tilde{m}$.

According to (10), the estimator $\widehat{\tilde{\vartheta}}$ is not the unbiased statistic of σ_N. For the analysis, suppose T samples with imprecise observations are available. For each sample batch, ML estimate of $\widehat{\tilde{\vartheta}}$ is obtained, then the mean of all collected sample groups will be:

$$\overline{\widehat{\tilde{\vartheta}}} = \frac{\sum_{i=1}^{T} \widehat{\tilde{\vartheta}_i}}{T} \tag{11}$$

Thus an unbiased estimator for σ_N can be developed as follows:

$$\hat{\sigma}_N = \frac{\overline{\widehat{\tilde{\vartheta}}}}{\delta} \tag{12}$$

Because the distribution of $\widehat{\tilde{\vartheta}}$ is highly skewed, particularly for smaller values of $\tilde{m}$, three-sigma limits are ordinarily inapplicable due to unequal tail sizes [36]. A common procedure in SPC is to use probability limits (PL) to address this issue. Since $\widehat{\tilde{\vartheta}}$ is followed by the χ_N distribution, its αt percentile is determined as:

$$F_{\chi_N}(\tilde{Z}) = \alpha \tag{13}$$

Using (8) in (13) yielded:

$$\widehat{\tilde{\vartheta}} = \frac{\sigma_N}{\sqrt{3\tilde{m}}} F_{\chi_N}{}^{-1}(\tilde{Z}) \tag{14}$$

As a result, the PL of the $\tilde{V}_{SQ}$-chart is constructed as follows:

$$upl_N = \frac{\sigma_N}{\sqrt{3\tilde{m}}} F_{\chi_N}{}^{-1}\left(1-\frac{\alpha}{2}\right) = \sigma_N \tilde{t}_1$$

$$lpl_N = \frac{\sigma_N}{\sqrt{3\widetilde{m}}} {F_{\chi_N}}^{-1}\left(\frac{\alpha}{2}\right) = \sigma_N \tilde{t}_2 \tag{15}$$

where $\tilde{t}_1 = \frac{{F_Y}^{-1}\left(1-\frac{\alpha}{2}\right)}{\sqrt{3\widetilde{m}}} = [t_{1l}, t_{1u}]$ and $\widetilde{t_2} = \frac{{F_Y}^{-1}\left(\frac{\alpha}{2}\right)}{\sqrt{3\widetilde{m}}} = [t_{2l}, t_{2u}]$ are neutrosophic values.

When the parameter defining the $\widetilde{\text{MD}}$ distributed quality characteristic is not provided, it is derived using an estimator described in (10). Thus the estimated PL becomes:

$$\widehat{upl}_N = \frac{\hat{\sigma}_N}{\sqrt{3\widetilde{m}}} {F_{\chi_N}}^{-1}\left(1-\frac{\alpha}{2}\right) = \bar{\tilde{\vartheta}}\tilde{t}_3$$

$$\widehat{lpl}_N = \frac{\hat{\sigma}_N}{\sqrt{3\widetilde{m}}} {F_{\chi_N}}^{-1}\left(\frac{\alpha}{2}\right) = \bar{\tilde{\vartheta}}\tilde{t}_4 \tag{16}$$

where $\tilde{t}_3 = \frac{{F_Y}^{-1}\left(1-\frac{\alpha}{2}\right)}{\delta\sqrt{3\widetilde{m}}} = [t_{3l}, t_{3u}]$ and $\tilde{t}_4 = \frac{{F_Y}^{-1}\left(\frac{\alpha}{2}\right)}{\delta\sqrt{3\widetilde{m}}} = [t_{4l}, t_{4u}]$

For a fixed of false alarm probability α and various values of m, the classic pair of crisp values $(\tilde{t}_1, \tilde{t}_2)$ and $(\tilde{t}_3, \tilde{t}_4)$ are easily computed and viewable in [31]. Three-sigma limits may be derived similarly but are not discussed in detail here due to the asymmetric form of the underlying statistic, particularly for the lower value of $\widetilde{m}$.

4. PERFORMANCE METRICS

The performance measures applied in this study are explained in this section. The suggested control charts' performance is assessed using a variety of metrics, however the average neutrosophic run length $(\widetilde{\text{ARL}})$ is the most frequently used and well accepted metric for analyzing neutrosophic control charts. The other related quantities such as neutrosophic power function $(\widetilde{\text{PF}})$ and neutrosophic characteristics function $(\widetilde{\text{CH}})$ are also described. The $\widetilde{\text{PF}}$ and $\widetilde{\text{CH}}$ functions are traditionally used to evaluate the sensitivity of the control chart to identify a sustained shift in key parameters. Whereas average number of neutrosophic points display on a control chart prior to the detection of an out-of-control signal is referred to as the $\widetilde{\text{ARL}}$. In this concept, it has been considered that samples are taken at evenly spaced time intervals. The $\widetilde{\text{ARL}}$ is actually the average value of the run-length distribution when the process is in-control (IC) and is usually denoted by $\widetilde{\text{ARL}}_0$. On the other hand, when a shift occurs, the number of samples collected from that point onward is known as out-of-control (OC) run length $(\widetilde{\text{ARL}}_1)$. Of course, the optimum circumstance for a given chart is for $\widetilde{\text{ARL}}_0$ to be large and $\widetilde{\text{ARL}}_1$ to be small. However, this is harder to establish, as it is with the Type-I and Type-II errors probabilities in the hypothesis test framework. As a remedy for this problem, the SPC literature employs an approach similar to hypothesis testing in which the $\widetilde{\text{ARL}}_0$ value is fixed at a certain level and the $\widetilde{\text{ARL}}_1$ value is reduced as much as feasible. To compute the value of $\widetilde{\text{ARL}}_1$, the ability of $\tilde{\text{V}}_{\text{SQ}}$-chart of not detecting the shift is given by:

$$\beta_N = P[lpl_N \leq \tilde{\vartheta} \leq upl_N / H_1] \tag{17}$$

Further simplification of (17) yielded:

$$\beta = F_{\chi_N}\left(\theta\tilde{\vartheta}_1\sqrt{3\tilde{m}}\right) - F_{\chi_N}\left(\theta\tilde{\vartheta}_2\sqrt{3\tilde{m}}\right) \tag{18}$$

where θ is the shift constant that linked the IC parameter with OC parameter as:

$$\tilde{\vartheta}_1 = \theta\tilde{\vartheta}_0;\ \tilde{\vartheta}_0 = \left[\tilde{\vartheta}_{l0}, \tilde{\vartheta}_{u0}\right] \tag{19}$$

Thus $\widetilde{ARL}_1$ can be defined as:

$$\widetilde{ARL}_1 = \frac{1}{1-F_{\chi_N}\left(\theta\tilde{t}_1\sqrt{3\tilde{m}}\right)+F_{\chi_N}\left(\theta\tilde{t}_2\sqrt{3\tilde{m}}\right)} = \frac{1}{1-\beta} \tag{20}$$

Note that the expression $1 - F_{\chi_N}\left(\theta\tilde{t}_1\sqrt{3\tilde{m}}\right) + F_{\chi_N}\left(\theta\tilde{t}_2\sqrt{3\tilde{m}}\right) = 1 - \beta$ establishes the $\widetilde{PF}$ of the proposed chart and when θ becomes equal to 1, (20) provides $\widetilde{ARL}_0$ i.e., mean of IC run length while the other values of θ i.e., $\theta \neq 1$, provides upwardly and downwardly shifts in the observed parameter of the proposed model. Now we compute the values of $\widetilde{ARL}_1$ and $\left(\widetilde{PF}\right)$ of the proposed chart for known value of process parameters. For this, we assume that $\tilde{m} = [3,5]$, crisp $\widetilde{ARL}_0 = [370, 370]$ and upwardly shift in the observed parameter. In such case, computed $\widetilde{ARL}_1$ and $\left(\widetilde{PF}\right)$ are depicted in Figure 4 and Figure 5, respectively.

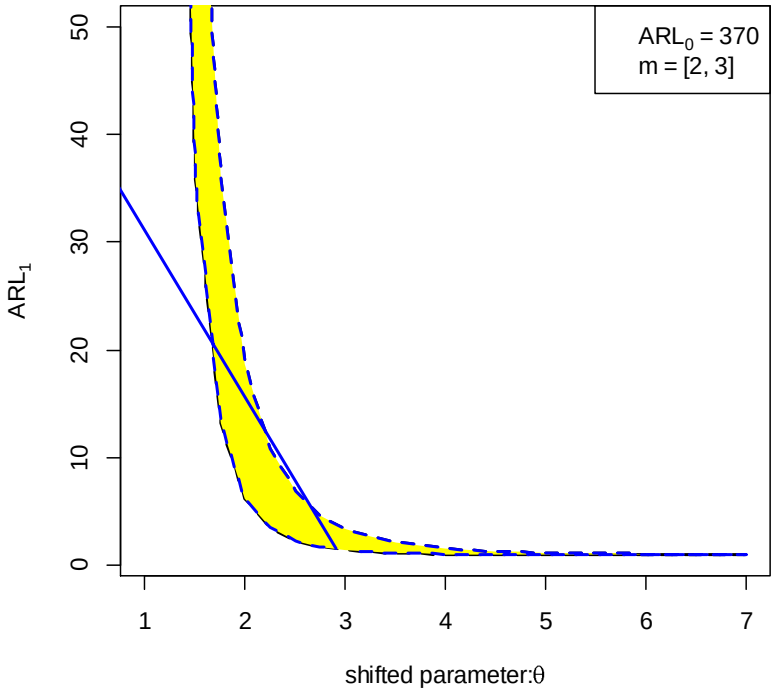

Figure 4 The $\widetilde{ARL}_1$ curve of the proposed $\tilde{V}_{SQ}$-chart

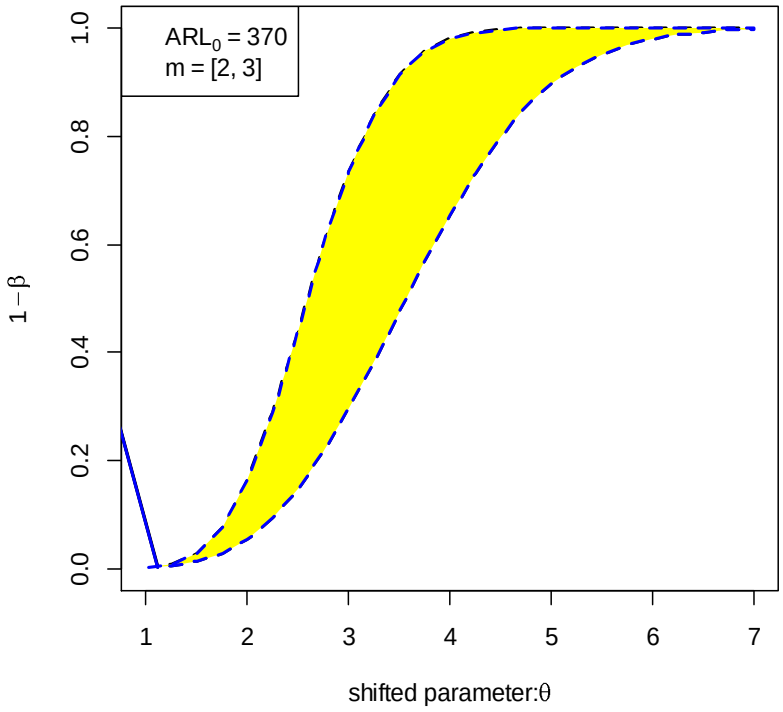

Figure 5 The $\widetilde{PF}$ curve of the proposed $\widetilde{V}_{SQ}$-chart

Figure 4 depicts the geometric shape of the RL distribution for a certain $\tilde{m}$, several curves may be graphed similarly for various $\tilde{m}$ values. It is clear from the graphs in Figure 4 that $\widetilde{ARL}_1$ drops as θ or $\tilde{m}$ grow. The graph in Figure 4 might be useful in determining the average interval number of samples required for a specific change in the study parameter. On the other hand, various changes in the observing parameter have been detected by the $\widetilde{V}_{SQ}$-chart as revealed in Figure 5. For example, the shifted amounts of $3\tilde{\vartheta}_0$ and $5\tilde{\vartheta}_0$ have been detected by the proposed chart with interval powers equal to [0.23, 0.42] and [0.85, 0.95], respectively. Thus as a conventional the $\widetilde{V}_{SQ}$-chart also detects the greater shifts with higher probabilities. In addition, we have provided the

performance of $\widetilde{V}_{SQ}$-chart in terms of $\widetilde{ARL}_1$ in Table 1. The results in Table 1 are based on 10^5 simulations of each shift in the study parameter at a fixed benchmark value $\widetilde{ARL}_0 = [370, 370]$.

Table 1 The estimated $\widetilde{ARL}_1$ of $\widetilde{V}_{SQ}$-chart

Shifting amount (θ)	Sample size		
	[2, 3]	[5, 7]	[9, 12]
1.00	[371.77,372.05]	[369.54,370.57]	[365.69,370.57]
1.25	[132.32,214.55]	[35.80,62.82]	[22.57, 35.80]
1.50	[35.88, 80.03]	[5.51, 11.62]	[3.27,5.51]
1.75	[13.23, 35.95]	[1.95, 3.81]	[1.36,1.95]
2.00	[6.18, 18.60]	[1.21, 1.91]	[1.04,1.21]
2.25	[3.47, 10.75]	[1.03, 1.30]	[1.00,1.03]
2.50	[2.27, 6.81]	[1.00, 1.09]	[1.00,1.00]
2.75	[1.67, 4.65]	[1.00, 1.02]	[1.00,1.00]
3.00	[1.36, 3.38]	[1.00,1.00]	[1.00,1.00]
3.25	[1.18, 2.60]	[1.00,1.00]	[1.00,1.00]
3.50	[1.18, 2.60]	[1.00,1.00]	[1.00,1.00]
3.75	[1.09,2.09]	[1.00,1.00]	[1.00,1.00]
4.00	[1.04, 1.75]	[[1.00,1.00]	[1.00,1.00]
4.25	[1.01, 1.52]	[1.00,1.00]	[1.00,1.00]
4.50	[1.00, 1.36]	[1.00,1.00]	[1.00,1.00]
4.75	[1.00, 1.25]	[1.00,1.00]	[1.00,1.00]
5.00	[1.00, 1.17]	[1.00,1.00]	[1.00,1.00]

Results in Table 1 show the performance of $\widetilde{V}_{SQ}$-chart at various neutrosophic sample sizes. It looks that estimated $\widetilde{ARL}_1$ is closer to the benchmark value of 370 when no shift occurred in the process parameter, i.e., $\theta = 1$. In contrast, for other values of θ, $\widetilde{ARL}_1$ steadily decreases as expected with an increase in the shifted parameter.

5. COMPARATIVE STUDY

In this section, the performance of the suggested chart is compared to that of other existing model utilized to monitor the parameter of interest of the Maxwell model. It has been evaluated against an existing model of the V-chart in an indeterminate framework to observe how well $\widetilde{V}_{SQ}$-chart performs. Various measures can be used for this comparison, although power curves are routinely employed in many research studies [37]–[39]. The equation (20) shows that power curve is a function of α, $\tilde{m}$ and θ. Power curves are often used to show the connection between these parameters. The development of the power curve for the suggested model is also based on the distribution of the estimator $\widetilde{\hat{\vartheta}}$. In estimating how large sample size is needed to detect an observable difference with a given probability, power curves can be helpful. In our case, the power of the $\widetilde{V}_{SQ}$-chart is defined as if the computed $\widetilde{\hat{\vartheta}}$ statistic surpasses the design limits for particular values of α and $\tilde{m}$. To construct the power curve, assume that $\tilde{\vartheta}_0$ is an IC value of the observed

process. Then $\widetilde{PF}$ indicates the likelihood of detecting a shift to a new value, say $\tilde{\vartheta}_1$, where $\tilde{\vartheta}_1 = \theta\tilde{\vartheta}_0$ on the first sample after the shift. This approach is used to evaluate the neutrosophic power of the recommended chart and its counterpart for fixed values of $\widetilde{ARL}_0$ and $\tilde{m}$ in Figure 6.

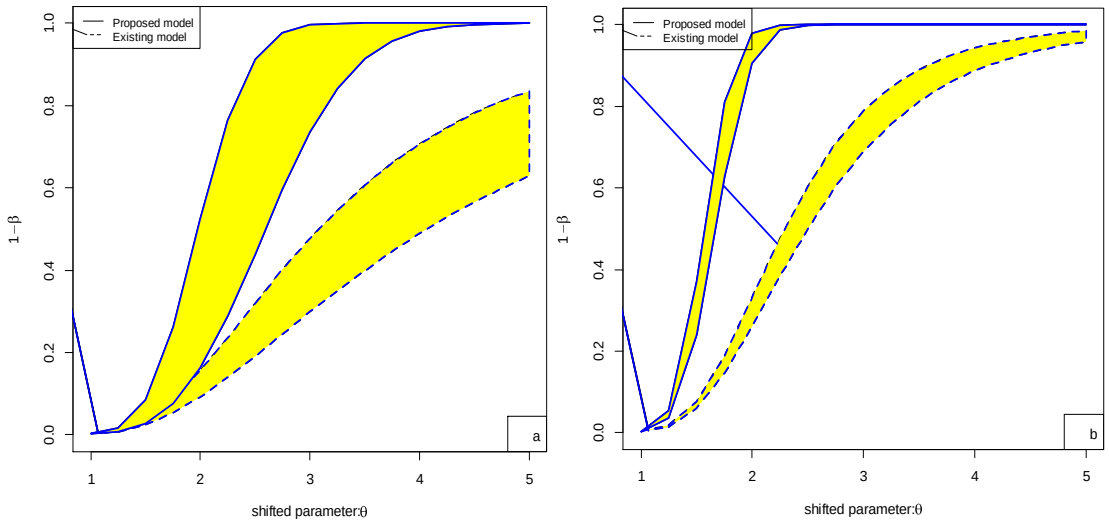

Figure 6 Power comparisons of $\tilde{V}_{SQ}$-chart at (a) $\widetilde{ARL}_0 = [370, 370]$ and $\tilde{m} = [3,5]$, (b) $\widetilde{ARL}_0 = [370, 370]$ and $\tilde{m} = [8,10]$

For examining Figure 6, it is observed that the suggested $\tilde{V}_{SQ}$-chart is particularly successful in identifying process changes even for small sample size. As an illustration, the power of $\tilde{V}_{SQ}$-chart and neutrosophic V-chart for detecting a shift of amount $3\tilde{\vartheta}_0$ are [0.75, 0.95] and [0.25, 0.40] respectively at $\tilde{m} = [3,5]$.Whereas the same comparison with higher probabilities hold for a larger sample size, i.e., $\tilde{m} = [8,10]$. Thus the proposed chart is deemed efficiently and highly sensitive for detecting the shift of different amounts in the studied parameter of the neutrosophic Maxwell process.

6. REAL-LIFE APPLICATION

In this section, a real-life example of the healthcare sector has been described to explain the theoretical framework of the proposed method. A patient's life or death is at stake in healthcare quality. To ensure patient satisfaction and safety, the healthcare system requires both investment and quality. Quality is a major concern for investors in this sector, which has seen a steady rise in investment. The assumption that the distribution of most medical data is normal is not accurate in most cases, so the customary assumption of normality approximation turns into inadequate for nonnormal data analysis. On the contrary, the techniques proposed in this work may effectively monitor and model the healthcare data. The capacity to reliably monitor the mean incubation time of COVID-19 and its variability in healthcare has become a major issue for the government,

industry, the general public, and academics. We have applied $\tilde{V}_{SQ}$-chart to COVID-19 mean incubation time data taken from the source [40] to examine the possible variability in incubation periods estimated from different studies. Being aware of the incubation period model while dealing with a point source pandemic enables statistical evaluation of exposure time. This information may also be used to evaluate hypotheses about whether the pandemic has come to an end by analyzing incubation time distribution during point-source epidemics. The incubation time, defined as the period between initial infection and illness manifestation, is an essential indicator for characterizing the spread of contagious diseases and developing quarantine policies [41]. It is important because reproduction numbers are often calculated using the mean incubation time, while quarantine durations are typically determined by using the maximum incubation period. The typical incubation time for COVID-19 varies widely, ranging from 3 days to 18 days [42]. As a result, it's impossible to quantify a precise quarantine period. Incubation periods have been found to vary widely in different research studies most likely because of the study population size and the estimating methodologies used. As a result, the mean incubation duration worldwide from the source is reported in Table 2 with uncertainties rather than precise figures in 12 subgroups.

Table 2: COVID-19 mean incubation period data with uncertainties

Sample batch	Mean incubation period values			
1	[7.81, 9.00]	[8.31, 9.16]	[4.48, 5.65]	[7.43, 8.51]
2	[4.95, 5.80]	[6.75, 7.62]	[5.05, 6.01]	[4.95, 5.22]
3	[6.49, 7.73]	[5.58, 6.45]	[5.55, 6.80]	[6.85, 7.18]
4	[3.99, 4.57]	[4.82, 5.04]	[6.58, 7.12]	[3.38, 4.45]
5	[8.94, 9.48]	[6.11, 7.60]	[5.36, 6.40]	[4.84, 5.05]
6	[5.35,6.63]	[9.48, 10.68]	[8.35, 9.27]	[7.93, 8.74]
7	[5.91, 6.16]	[9.90, 10.50]	[10.31, 11.37]	[8.32, 8.92]
8	[5.21, 5.98]	[5.88, 6.68]	[5.03, 5.31]	[3.83, 5.18]
9	[5.82, 6.90]	[6.01, 7.01]	[5.07, 6.14]	[2.52, 3.73]
10	[7.38, 8.18]	[5.80, 7.26]	[6.76, 7.57]	[6.52, 7.70]
11	[6.32, 6.86]	[5.33, 6.78]	[5.07,5.77]	[2.07, 3.65]
12	[7.42, 8.21]	[4.06, 5.92]	[4.17,5.48]	[3.72, 4.52]

Mean incubation time uncertainties are introduced to the technique devised in [13]. An informal graphical approach has shown that the Maxwell distribution is an acceptable model for representing the incubation time data since most actual data does not stray greatly from the theoretical red lines. The process data are skewed, as seen from the histogram and CDF plot in Figure 7 and Figure 8. As a result, the data may be further examined using the model that has been suggested.

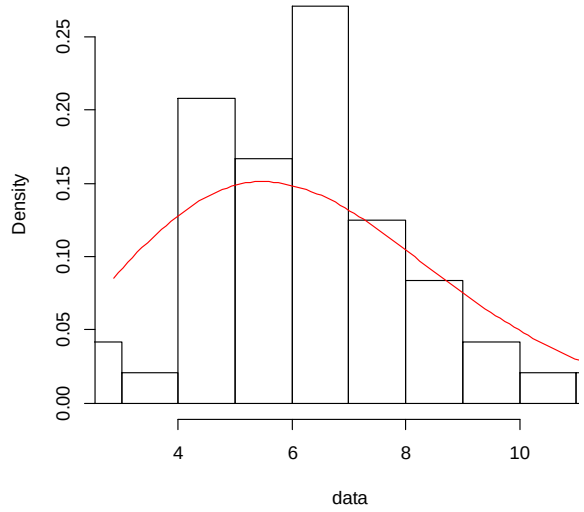

Figure 7. Histrogram of COVID-19 incubation period data

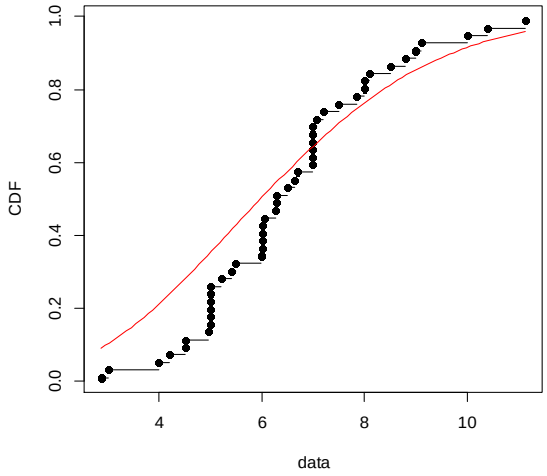

Figure 8. Theoretical and empirical CDF plots of incubation period data

By considering the individual values given in Table 2, the ML estimator $\widehat{\tilde{\vartheta}}$ can be obtained from each subgroup in Table 3:

Table 3: Neutrosophic estimates of the proposed model for each sample group

Sample batch	Neutrosphic estimator $\left(\widehat{\tilde{\vartheta}}\right)$
1	[4.14, 4.73]
2	[3.16, 3.59]
3	[3.54, 4.07]
4	[2.79, 3.12]
5	[3.75, 4.22]
6	[4.52, 5.16]
7	[5.06, 5.45]
8	[2.91, 3.36]
9	[2.92, 3.52]
10	[3.83, 4.44]
11	[2.86, 3.41]
12	[2.92, 3.56]

After finding ML estimate of $\widehat{\tilde{\vartheta}}$ from each sample batch, the mean of all collected sample groups from (10) can be obtained as:

$$\overline{\widehat{\tilde{\vartheta}}} = [3.54, 4.06]$$

The upper and lower probability limits for sample size 4 utilizing (16) thus can be obtained as:

$\widehat{\text{upl}}_{\text{N}} = \max[5.90, 6.78]$ and $\widehat{\text{lpl}}_{\text{N}} = \min[1.60, 1.80]$.

The proposed control chart based on these limits is depicted in Figure 9.

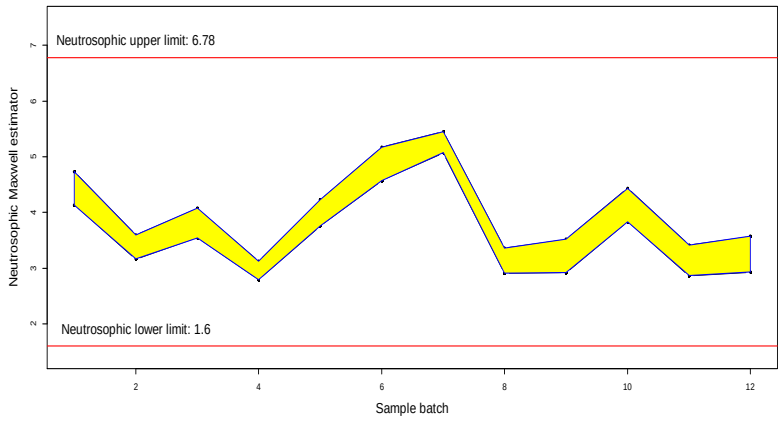

Figure 9. Control chart based on the proposed model

The depicted Maxwell estimator in Figure 9 exhibits a random tendency within the control limits. Thus, observable data-generating mechanisms may be inferred as a statistical control condition.

.

7. CONCLUSIONS

The classical Maxwell model under the neutrosophic logic has been extended in this work. Several theoretical aspects of the proposed $\widetilde{\mathrm{MD}}$ distribution, such as its probability density function, characteristic function, and a few raw moments, are investigated. The theoretical framework of the suggested model, notably in domains of SPC, have been described for working data, including ambiguous, indeterminate, and imprecise observations on examined variables. Because of its suitability for dealing with ambiguous data in SPC applications, a new control chart based on the suggested $\widetilde{\mathrm{MD}}$ distribution has been developed. Some essential charting characteristics such as power curve $(\widetilde{\mathrm{PC}})$, the neutrosophic characteristic curve $(\widetilde{\mathrm{CC}})$ and neutrosophic run length $(\widetilde{\mathrm{RL}})$ of the proposed chart in terms of neutrosophic logic have been derived and validated through simulated data. A simulation study is carried out to demonstrate the theoretical results and the effectiveness of the $\widetilde{\mathrm{V}}_{\mathrm{SQ}}$-chart is evaluated to that of existing counterparts. Simulation results reveal that the proposed chart is deemed efficiently and have highly discriminatory power for detecting the shift of different amounts in the studied parameter of $\widetilde{\mathrm{MD}}$ distribution. Finally, the usefulness of the $\widetilde{\mathrm{V}}_{\mathrm{SQ}}$-chart has been described considering the real data example on the incubation period of COVID-19. Based on the results given in this study, neutrosophic extension may be designed for other statistical models in future work.

Funding: This research received no external funding

Conflicts of Interest: The authors declare no conflict of interest.

REFERENCES

1 P. Qiu, Some perspectives on nonparametric statistical process control, *J. Qual. Tech.,* 2018, vol. 50, no. 1, pp. 49–65.

2 G. Suman and D. R. Prajapati, Control chart applications in healthcare: a literature review, *Int. J. Metrol. Qual. Eng.*,2018, vol. 9, p. 5.

3 N. Imam, T. Spelman, S. A. Johnson, and L. J. Worth, Statistical process control charts for monitoring staphylococcus aureus bloodstream infections in australian health care facilities, *Qual. Manag. Health Care*, 2019, vol. 28, no. 1, pp. 39–44.

4 C. Shi and L. Rothrock, Validating an abnormal situation prediction model for smart manufacturing in

the oil refining industry, *Appl. Ergon.*,2022, vol. 101, p. 103697.

5 M. Abid, S. Mei, H. Z. Nazir, M. Riaz, and S. Hussain, A mixed HWMA-CUSUM mean chart with an application to manufacturing process, *Qual. Reliab. Eng. Int.*, 2021, vol. 37, no. 2, pp. 618–631.

6 R. J. Perla, S. M. Provost, G. J. Parry, K. Little, and L. P. Provost, Understanding variation in reported covid-19 deaths with a novel Shewhart chart application, *Int. J. Qual. Heal. Care*, 2021,vol. 33, no. 1, mzaa069.

7 Z. J. Viharos and R. Jakab, Reinforcement learning for statistical process control in manufacturing, *Measurement*, 2021, vol. 182, p. 109616.

8 I. Madanhire and C. Mbohwa, Application of statistical process control (SPC) in manufacturing industry in a developing country, *Procedia CIRP*, 2016, vol. 40, pp. 580–583.

9 Í. L. Ansorena, Statistical process control and quality of service at seaports, *Int. J. Product. Qual. Manag.*, 2018, vol. 24, no. 2, pp. 165–176.

10 I. M. Zwetsloot and W. H. Woodall, A review of some sampling and aggregation strategies for basic statistical process monitoring,, *J. Qual. Tech.,2019,* vol. 53, no. 1, pp. 1–16.

11 M. Aslam, R. A. R. Bantan, and N. Khan, Design of a new attribute control chart under neutrosophic statistics, *Int. J. Fuzzy Syst.*, 2019, vol. 21, no. 2, pp. 433–440.

12 D. Hoffman and O. J. Karst, Theory of the Rayleigh distribution and some of its applications, *J. Sh. Res.*, 1975, vol. 19, no. 03, pp. 172–191.

13 Z. Khan, M. Gulistan, R. Hashim, N. Yaqoob, and W. Chammam, Design of S-control chart for neutrosophic data: An application to manufacturing industry, *J. Intell. Fuzzy Syst.*, 2020, vol. 38, no. 4, pp. 4743–4751.

14 Z. Khan, M. Gulistan, W. Chammam, S. Kadry, and Y. Nam, A new dispersion control chart for handling the neutrosophic data, *IEEE Access*, 2020, vol. 8, pp. 96006–96015.

15 A. Faraz and M. Bameni Moghadam, Fuzzy control chart a better alternative for shewhart average chart, *Qual. Quant.*, 2007, vol. 41, no. 3, pp. 375–385.

16 M. Aslam and M. A. Raza, Design of new sampling plans for multiple manufacturing lines under uncertainty, *Int. J. Fuzzy Syst.*, 2019, vol. 21, no. 3, pp. 978–992.

17 M. Gülbay, C. Kahraman, and D. Ruan, α-cut fuzzy control charts for linguistic data, *Int. J. Intell. Syst.*, 2004, vol. 19, no. 12, pp. 1173–1195.

18 M. Hossein, Z. Sabegh, A. Mirzazadeh, S. Salehian, and G.-W. Weber, A literature review on the fuzzy control chart; classifications & analysis, *Int. J. Supply Oper. Manag.*, 2014, vol. 1, no. 2, pp. 167–189.

19 Z. Khan, M. Gulistan, N. Kausar, and C. Park, Neutrosophic Rayleigh model with some basic characteristics and engineering applications, *IEEE Access*, 2021, vol. 9, pp. 71277–71283.

20 Prem Kumar Singh, Complex Plithogenic Set, International Journal of Neutrosophic Science, Vol. 18 , No. 1

21 Z. Khan, A. Al-Bossly, M. M. A. Almazah, and F. S. Alduais, On statistical development of neutrosophic gamma distribution with applications to complex data analysis, *Complexity*, vol. 2021.

22 F. Smarandache *et al.*, Introduction to neutrosophy and neutrosophic environment, *Neutrosophic Set Med. Image Anal.*,2019, pp. 3–29.

23 F. Smarandache, Neutrosophical statistics. Sitech & Education publishing, 2014..

24 M. Aslam, Analyzing wind power data using analysis of means under neutrosophic statistics, *Soft Comput.*, 2021, vol. 25, no. 10, pp. 7087–7093.

25 Z. Khan *et al.*, Statistical development of the neutrosophic lognormal model with application to environmental data, *Neutrosophic Sets Syst.*, vol. 47, 2021.

26 E. H. Marcia Esther , F. H. Robert Alcides , P. P. Rene Estalin, Neutrosophic Statistics for Social Science, International Journal of Neutrosophic Science, Vol. 19 , No. 1 , (2022) : 250-259

27 M. A. U. Haq. A new Cramèr–von Mises Goodness-of-fit test under Uncertainty, *Neutrosophic Sets and Systems*, vol. 49, no.1, p.16, 2022.

28 M. A. U. Haq. Neutrosophic Kumaraswamy Distribution with EngineeringApplication, *Neutrosophic Sets and Systems*, vol. 49, no.1, p.17, 2022.

29 R. A. K. Sherwani, M. Aslam, M. A. Raza, M. Farooq, M. Abid, and M. Tahir, Neutrosophic normal probability distribution—a spine of parametric neutrosophic statistical tests: properties and applications, *Neutrosophic Oper. Res.*,2021, pp. 153–169.

30 Z. Khan, M. Gulistan, S. Kadry, Y. Chu, and K. Lane-Krebs, On scale parameter monitoring of the Rayleigh distributed data using a new design, *IEEE Access*,2020, vol. 8, pp. 188390–188400.

31 M. Aslam, R. A. R. Bantan, and N. Khan, "Design of a new attribute control chart under neutrosophic statistics," *Int. J. Fuzzy Syst.*, 2019, vol. 21, no. 2, pp. 433–440.

32 M. P. Hossain, M. H. Omar, and M. Riaz, New V control chart for the Maxwell distribution, *J. Stat. Comp., Simul.*, 2016, vol. 87, no. 3, pp. 594–606.

33 F. Shah, Z. Khan, M. Aslam, and S. Kadry, Statistical development of the VSQ -control chart for extreme data with an application to the carbon fiber industry, *Math. Probl. Eng.*,2021, vol. 2021.

34 V. K. Sharma, H. S. Bakouch, and K. Suthar, An extended Maxwell distribution: Properties and applications, *Simul Comput.,2017,* vol. 46, no. 9, pp. 6982–7007.

35 S. K. Tomer and M. S. Panwar, A Review on Inverse Maxwell Distribution with Its Statistical Properties and Applications, *J. Stat. Theory Pract.*, 2020, vol. 14, no. 3, pp. 1–25.

36 M. Xie and T. N. Goh, The use of probability limits for process control based on geometric distribution, *Int. J. Qual. Reliab. Manag.*, 1997, vol. 14, no. 1, pp. 64–73.

37 L. Zhang, K. Govindaraju, M. Bebbington, C. Lai, and C. D. Lai, "On the Statistical Design of Geometric Control Charts, vol. 1, no. 2, pp. 233–243, Qual. *Techn. Quant. Manag.*, 2016.

38 Juanjuan Ding , Wenhui Bai , Chao Zhang, A New Multi-Attribute Decision Making Method with Single-Valued Neutrosophic Graphs, International Journal of Neutrosophic Science, vol. 11 , No.2 , (2020) : 76-86

39 R. Mehmood, M. Riaz, and R. J. M. M. Does, "Control charts for location based on different sampling schemes,", vol. 40, no. 3, pp. 483–494, *J. Appl. Stat.,* 2013.

40 C. Cheng *et al.*, The incubation period of COVID-19: a global meta-analysis of 53 studies and a Chinese observation study of 11 545 patients, *Infect. Dis. Poverty*, 2021, vol. 10, no. 1, pp. 1–13.

41 K. Ejima *et al.*, "Estimation of the incubation period of COVID-19 using viral load data," *Epidemics*, 2021, vol. 35, p. 100454.

42 S. Lei *et al.*, Clinical characteristics and outcomes of patients undergoing surgeries during the incubation period of COVID-19 infection, *EClinical Medicine*, 2020, vol. 21, p. 100331.

Received: Sep 1, 2022. Accepted: Dec 18, 2022